Composites: Part A 165 (2023) 107328

Contents lists available at ScienceDirect

Composites Part A

journal homepage: www.elsevier.com/locate/compositesa

Programmable shape memory bismaleimide composite claw with two-way grabbing function

Yuejia Li [a], Fenghua Zhang [a,*], Yanju Liu [b], Jinsong Leng [a,*]

[a] Centre for Composite Materials and Structures, Harbin Institute of Technology (HIT), Harbin 150080, People's Republic of China
[b] Department of Astronautical Science and Mechanics, Harbin Institute of Technology (HIT), No. 92 West Dazhi Street, PO Box 301, Harbin 150001, People's Republic of China

ARTICLE INFO

Keywords:
A. Smart materials
A. Thermosetting resin
A. Polymer-matrix composites (PMCs)
B. Mechanical properties

ABSTRACT

Functional polymer materials with a two-way shape memory effect (2 W-SME) have attracted great interest recently. Herein, by introducing 2,4-tolylene diisocyanate (TDI) into the bismaleimide (BMI) network, the shape memory polymers we synthesized are a series thermosetting polymers with adjustable T_g and triple-shape memory effect(triple-SME), and realized two-way behavior by programming. Those shape memory polymers (SMPs) were toughened by acrylonitrile-butadienerubber (ETBN) and reinforced with carbon fabric to make composites. The cured network with varying transition temperatures and flexibility was synthesized by varying the cyanate ester and rubber concentration in the system. Polymers with a broad glass transition temperature (T_g) range can achieve triple-SME. Due to the complex cross-linked structure, the two-way behavior demonstrated above for BMI-based SMPs stem from its broad T_g ranges. Select two temperatures higher and lower than T_g as the switching temperature, and fix the pre-deformed shape in the opposite direction at these two temperatures to achieve the two-way behavior. These BMI-based SMPs could grab objects through the design of the structure. Results indicated that the above BMI-based SMPs with two-way function have excellent thermal stability and mechanical properties, which provides the basic attempts for the further development of thermosetting SMPs and their composite materials.

1. Introduction

Shape memory polymers (SMPs) are a kind of functional polymer materials, which have the ability to fix temporary shapes. Under external stimulation conditions such as temperature, light, electricity, magnetism, solvent and pH, the shape of SMPs will change positively [1–8]. The chemical cross-linking point or physical crystalline phase in SMP makes it have a fixed original shape. When the temperature is rised to the transition temperature (T_t), the non cross-linking point or crystalline phase is no longer fixed, and the shape of SMP can be changed by applying external force. By lowering the temperature below T_t to 'freeze' the chains in SMP, the obtained shape is a pre-deformed temporary shape [9]. Reheated to above T_t or stimulated by other particular conditions, the polymer segments relaxed and the materials can deform autonomously to the original shape. Thermosetting SMP is a kind of SMP with covalent cross-linking network, rather than semi-crystalline thermoplastic SMP. Compared with thermoplastic SMPs, the stable performance during the glass state and the flexibility during an elastomeric state of thermosetting SMPs make them have attractive characteristics [10–13]. They also show high response speed, low creep, high shape fixation and recovery rate [14–16]. Those thermosetting polymers with shape memory effect are widely used in biomedical field, intelligent robot field and deployable space structure field, and will have more attractive applications in the near future [17–22].

The phenomenon that SMP can be temporarily fixed into other shapes and recovery to the original shape is called shape memory effect (SME), which is also called dual shape memory effect (dual-SME) and one-way shape memory effect (1 W-SME). SMPs with the function of memorizing two or even more temporary shapes are called multi-shape memory polymers (multi-SMPs), which have multi-shape memory effects (multi-SME) [23]. Thermoplastic multi-SMPs have been systematically reported in recent years [24–26]. Thermosetting SMPs with multi-SME needs more research and development. Bellin *et al.* first reported a triple-SMP system by the blending of two polymer network systems, MACL contains poly(ε-caprolactone) (PCL) and poly(cyclohexyl methacrylate) ((PCHMA) and CLEG contains PCL and PEG

* Corresponding authors.
E-mail addresses: fhzhang_hit@163.com (F. Zhang), lengjs@hit.edu.cn (J. Leng).

https://doi.org/10.1016/j.compositesa.2022.107328
Received 25 July 2022; Received in revised form 6 November 2022; Accepted 15 November 2022
Available online 19 November 2022

Table 1
Details of BMI-based SMPs synthesis.

Sample no.	SMP1	SMP2	SMP3	SMP2-1	SMP2-2	SMP2-3
Mole fraction of BDM: D400:TDI	1:1:1	1:1:1.25	1:1:1.5	1:1:1.25	1:1:1.25	1:1:1.25
ETBN to BMI mass ratio (%)	0	0	0	2.5	5	10

monomethylether-monomethacrylate [27]. The transition temperature can be adjusted by adjusting the monomer ratio of CLEG. Mather *et al.* prepared triple-SMP by mixing materials with different T_g [28,29]. After epoxy resin and PCL are mixed, a phase separation structure is formed on the micro level. The polymer formed has a triple-SME. Xie *et al.* reported a polymer with bilayer structure by compounding two layers of epoxy resins with different glass transition temperatures (T_g) [30]. The shape memory performance of this material can be adjusted by adjusting the proportion of the two layers. Li *et al.* also observed a weak triple-SME on their SMP with narrow T_g [31,32]. At present, the thermosetting part of triple-SMPs have higher modulus compared to thermoplastic ones. But these thermosetting SMPs easily leads to brittle fracture failure during the folding and unfolding process [33].

To improve toughness and deformability, linear aliphatic or segments containing flexible groups are usually added to thermosetting molecules to prepare intrinsic toughened thermosetting SMP. However, the increase in toughness often leads to the decline of thermal and mechanical properties. To overcome the shortcomings of low strength of SMP, researchers used fibers (carbon fiber, glass fiber), suspended carrier (graphene, carbon nanotubes, carbon black, nickel powder) and hybrid carrier (carbon nanofiber/carbon nanopaper, nano silver particles/carbon black, nano aluminum powder/carbon fiber) to improve the mechanical properties, thermal conductivity and electrical conductivity of thermosetting SMP. Bismaleimide (BMI) resin is a kind of thermosetting and high temperature usable resin, which performed high strength and high T_g than typical epoxy resin and phenolic resin [34]. However, the BMI-based material is relatively brittle, and it is difficult to meet the vibration and other tests in the aerospace field. Biju *et al.* prepared BMI-based SMP composites using BMI resin with methyl-ethyl-ketone impregnated carbon fabric and molded in hot-press machine [35]. Transition temperature and flexural strength can be regulated by varying BMI-PTMO (BMI-end-capped poly (tetramethyleneoxide)) content. 2 W-SMPs so far are generally thermoplastic materials with low T_g, low temperature resistance and insufficient strength. Existing BMI-based SMPs with better strength do not have 2 W-SME and the production process of composites is complex. Making composites with high strength, high temperature resistance, appropriate toughness and 2 W-SME is a huge challenge.

In our study, the BMI-based SMPs with two-way function have higher T_gs. The use of chain extender polyether diamine poly(propyleneglycol) bis(2-aminopropylether) (D400) and crosslinking agent 2,4-tolylene diisocyanate (TDI) helps to improve the toughness of the SMPs fundamentally. The addition of liquid nitrile rubber (ETBN) increases the toughness of the SMPs. Complex covalent crosslinks give SMPs wide T_g ranges. This property allows these SMPs to remember two pre-deformed shapes. By designing the second pre-deformed shape similar to the original shape, the two-way behavior can be realized. The introduction of carbon fabric reinforced the claw structure, which can grab objects. This claw can be used as telescoping structures in space and other fields.

2. Experimental section

2.1. Materials synthesis

All the samples of the systems were synthesized using various reagents in different ratios, as shown in Table 1. 4,4′-Bismaleimidodiphenylmethane (BDM), a polyether diamine, amino-terminated polyoxypropylene (D400) (Mw = 400 g·mol^{-1}) and 2,4-tolylene diisocyanate (TDI) were purchased from Aladdin Co.. The epoxy-terminated liquid acrylonitrile-butadienerubber TGE32 (ETBN) was purchased from Suzhou Junxin Plastic Co., China. The chemical structures of BDM, D400, TDI and ETBN were illustrated in Fig. 1(i-iv), respectively. T300-type twill carbon fibric was from Toray Industries. All the chemicals used in the experiments are analytical grade and were used without further purification.

The synthetic process shown in Fig. 1 could be separated into three steps. First, dissolve calculated amount of BDM and D400 in solvent tetrahydrofuran and put the solution into a three-neck flask for reaction, as shown in Fig. 1a. During the reaction, argon is introduced to protect the reaction, and the outlet-neck is condensed to prevent excessive solvent volatilization. The flask was heated to 65 °C and the solution was stirred with mechanical stirrer. This is the method described in reference [36] to synthesize the linear backbone structure. As shown in Fig. 1a, the red and green lines represent the linear backbone structure, and the yellow dot represents the cross-linking point. After 24 h, the solution changes from bright yellow-colored to amber-colored. Second, add a certain proportion of TDI and NBR to the solution for stirring, as shown in Fig. 1b. After 5 min, pour the evenly stirred solution into the mold and dry it at room temperature (R.T.) for 24 h, as shown in Fig. 1C. After the introduction of TDI, a rubbery polymeric system was formed. The latter cross-linking point is expressed in brown, and the plasticizer NBR is shown in blue. After drying, place the mold and elastic material in the oven and cured at 60 °C for 2 h, 120 °C for 2 h, and 200 °C for 1 h, as shown in Fig. 1(c). Finally, a series of BMI-based SMPs with different cross-linking densities were obtained after cooling.

2.2. Preparation of BMI-based composites

As for the preparation of composites, the mentioned viscous solution was poured on the carbon fabric. The solvent was volatilized at room temperature until the solid content of the resin was about 50 %. The sticky fiber prepregs obtained were stacked together, and then molded into the required shape through the mold. The molded structure was placed in a 60 °C oven until completely dry and then the post-curing process was performed. Two, three and four layer carbon fabric BMI-based SMP composite samples and composite grabbing structures were obtained. The samples cut along the 0/90° direction of the carbon fabric are named SMPC-90–2, SMPC-90–3 and SMPC-90–4 respectively. The samples cut along the ± 45° direction of the carbon fabric are named SMPC-45–2, SMPC-45–3 and SMPC-45–4 respectively.

2.3. Characterization

Spectrum One (Perkin-Elmer, MA, USA) with the accessory of universal attenuated total refraction (ATR) were used to test the FTIR spectra, and study the vibration of functional groups in molecules. The wavelength range used is 4000–650 cm^{-1} with a resolution of 4 cm^{-1}.

Crosslinking density is characterized by swelling test. About 0.2 g sample is weighed, with the weight recorded as m_1. The weighed sample was put into sufficient deionized water or toluene, chloroform, DMAc. After two days, the solvent on the sample surface was wiped clean. The weight of dried sample was record as m_2. Swelling degree is calculated by Eqs. (1).

$$Swellingdegree = \frac{m_2 - m_1}{m_1} \times 100\% \quad (1)$$

Thermogravimetric analyzer (TGA) were used on Mettler-Toledo TGA/DSC STARe System under a N_2 flow environment from 25 to 800 °C at the heating rate of 10 °C min^{-1}, to get the thermal changes and the thermal stability of BMI-based SMPs.

The static mechanical properties were conducted by uniaxial tensile test on a Zwick electronic universal material testing machine at a rate of

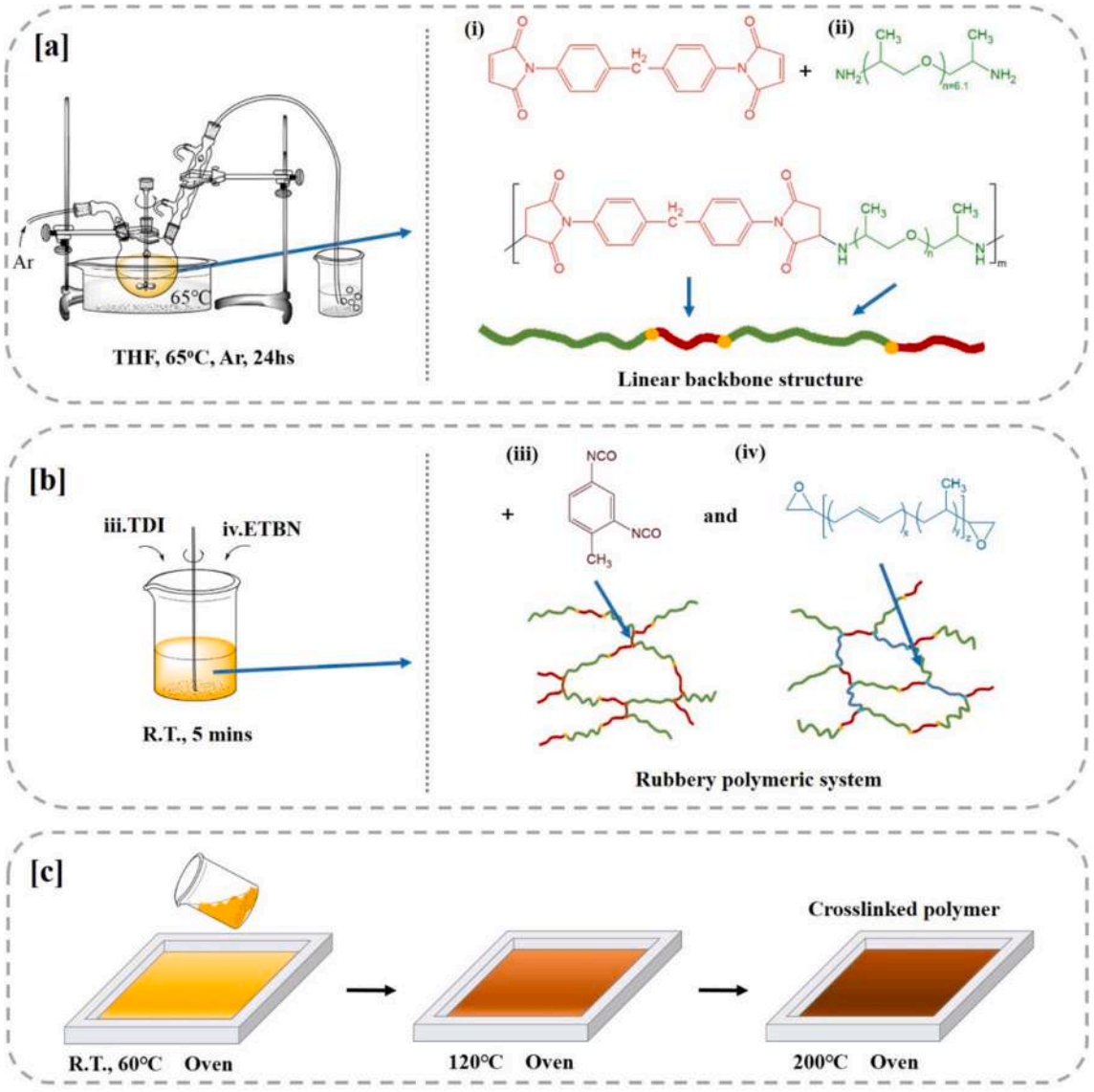

Fig. 1. Synthesis of (a) linear backbone structure, (b) rubbery polymeric system, (c) BMI-based SMPs. (i) 4,4′-bismaleimidodiphenylmethane (BDM), (ii) poly (propylene glycol) bis(2-aminopropyl ether) (D400), (iii) 2,4-tolylene diisocyanate (TDI) and (iv) epoxy-terminated liquid acrylonitrile-butadienerubber (ETBN).

1 mm/min at R.T.. ASTM-D 882–10 and ASTM-D638 Type-V were used as the test standards for BMI-based SMPs and composites, respectively. Scanning electron microscope (SEM) was used to observe the fracture morphology of sputtering gold plating sample.

The dual-SME tests were characterized by visual bending tests. A sample with a dimension of 30 × 5 × 1 mm^3 was folded to a U shape at $T_g + 20$ °C and fixed at room temperature. The angle of holding load and after unloading were recorded. The recovered temporary shape was obtained after heating to T_g + 20 °C. The angle after recovery was recorded.

Consecutive shape memory cycles were carried out by DMA. A sample with a dimension of 30 × 4 × 1 mm^3 was used in this test. The sample was clamped by the tensile mode clamp. First, it was heated to T_g. After heat preservation, sample was stretched. Under the condition of maintaining 4–8 N tensile force, the sample was cooled to room temperature. After unloading, it was heated to T_g again. Finally, it was cooled to room temperature to end a cycle. Each sample was cycled five times. Shape fixation rate (R_f) is calculated by Eqs. (2). Shape recovery rate (R_r) is calculated by Eqs. (3).

$$R_f(\%) = \frac{\varepsilon_{fix}}{\varepsilon_{deform}} \times 100\% \tag{2}$$

$$R_r(\%) = \frac{\varepsilon_{deform} - \varepsilon_{recover}}{\varepsilon_{deform} - \varepsilon_{initial}} \times 100\% \tag{3}$$

where ε_{deform} and ε_{fix} represent the fixed strain after cooling and load removal, respectively; $\varepsilon_{initial}$ and $\varepsilon_{initial}$ ndicate the strain before loading and the strain after recovery for each shape, respectively.

3. Results and discussion

3.1. ATR-FTIR analysis of BMI based SMPs chemical structure

The vibration of functional groups of the BMI-based SMPs were characterized by ATR-FTIR analysis. Fig. 2(b) shows the main characteristic peaks 1709 cm^{-1} (carbonyl) and 1175 cm^{-1} (C—N—C) of the

series of materials. The figure also shows 2967 cm^{-1} ($–CH_3$) and 2871 cm^{-1} ($–CH_2$-) peaks. The $–CH_3$ group is from BDM and D400, the $–CH_2$ group is from D400. The peaks at 2275 cm^{-1} and 2237 cm^{-1} which are belonging to cyanate ester disappear completely. It indicates that cyanate ester group reacted with secondary amine group in the main chain. There is no peak of 1564 cm $^{-1}$ and 1366 cm^{-1} belonging to the triazine ring. This reaction fabricated the first kind of crosslinking points. It can be seen from Figure S1 that with the increase of cross-linking agent content, the swelling degree of sample SMP1 to SMP3 gradually decreases, which indicates that the cross-linking density gradually increases[37,38]. It can be seen in Fig. 2(a) that the colors of SMP3 are more profound than that of SMP1. The peak at 1464 cm^{-1} represents the disappearance of methylene. This states that further crosslinking reaction occurs, forming another kind of crosslinking point. Different crosslinking structures show different widths and peaks of T_g peak, and this complex homogeneous crosslinking network shows the superposition of different T_g peaks, realizing a wide glass transition temperature range, and then realizing the multi-shape memory effect. As shown in Fig. 2(c), there is no obvious change after adding nitrile rubber, indicating that nitrile rubber does not undergo relevant reaction. At the same time, it can be seen from Figure S1 that the swelling degree of samples SMP2-1 to SMP2-2 gradually increases, and the crosslinking density gradually decreases [37,38]. This shows that the addition of rubber reduces the crosslinking density of the material.

3.2. Thermal performance analysis

Thermal stabilities of the BMI based TSMPs with different proportions were investigated by TGA in the nitrogen atmosphere from 25 °C to 800 °C at a heating rate of 10 °C min^{-1}. Fig. 3(a) and Fig. 3(b) show the thermogravimetric curves of BMI-based SMPs with different mixture ratios and SMPs with different nitrile rubber ratios. The temperatures of minimal (<5%) decompositions (T_d) for all examined samples are above 250 °C, which are higher than the T_g of the materials. It demonstrates that the BMI-based SMPs can be used durably in their operating temperature ranges without significant thermal degradation. There is a slight increase in the residual weight of SMP3, which is caused by the higher crosslinking degree [39]. SMP2-3 shows the fastest decomposition rate indicates that the added rubber segments are easier to decompose. SMP2-3 also shows the lowest residue weight, as the more rubber, the lower crosslinking degree of the system. Due to the same type of chemical bonds, all the samples showed major decompositions at about 400 °C. Therefore, this approach is an appropriate method to achieve triple-shape memory ability without the sacrifice of thermal stabilities of thermosetting SMPs.

Fig. 3(c) shows the thermogravimetric test curve of SMP2-2 based composites and SMP2-2. Based on the fact that the carbon fiber in the composite does not decompose below 800 °C, the resin content and carbon fiber content in the composite were calculated through the data of thermogravimetric analysis. The weight loss of composites and SMPs can be calculated from the remaining weight. The resin content in the composite can be obtained by dividing the weight of composites at 800 °C by the weight loss of SMPs at 800 °C. The resin contents of SMPC-90-2, SMPC-90-3 and SMPC-90-4 were 70 %, 59 % and 41 %, respectively. This indicates that the composites exhibit adequate resin content. And it shows a trend of the more composite layers, the lower resin content. Under the same thickness, the higher the fiber content, the lower the resin content.

3.3. Dynamic mechanical analysis

The DMA curves of storage modulus and tan δ can be seen in Fig. 4. These curves represents the relationship between the stiffness of the material and temperature. The modulus of SMPs and composites in glass state ($E_{25°C}$), intermediate state ($E_{Tg\text{-}40°C}$) and rubber state ($E_{Tg+40°C}$) are summarized in Table 2. In the low temperature range, the samples all present high modulus and glassy plateau. In the high temperature range, the samples all show low modulus and rubber plateau. Between the two plateaus, the storage modulus of the material decreases sharply and covers a certain temperature range, which shows a relatively wide width. If the modulus of the material decreases to a certain extent, it can prove that the material has the shape memory effect. The wide temperature range of modulus decline proves that these materials have the ability of multi-shape memory effect. With the increase of BACE content, the crosslinking density of the material is higher, showing higher storage modulus and T_g, as shown in Fig. 4(a). *Tan* δ is the relative ratio of the loss modulus to the storage modulus, which can be used to evaluate the energy dissipation in materials. In the field of shape memory materials, tan δ is also used to represent the estimated value of T_g. The resulting estimated T_g values of the materials are listed in Table 2. And it can be seen from the figures that there is no obvious correlation between the width of tan δ peak of the materials and the crosslinking density of the materials. These SMPs possesses a broad glass transition exceeding 50 °C. SMPs with broad glass transitions show a triple-shape memory effect. The broad tan δ peak indicates that it is the superposition of multiple T_g peaks, which means that the material is a cross-linked network with heterogeneous structures [40]. The DMA curves of SMPs with different ETBN ratios are shown in Fig. 4(b). To increase the toughness of SMP2, ETBN was added to connect with the backbone structure. The more ETBN is added, the lower T_g and storage modulus of the material. The reason is that the segment flexibility of the rubber chain is high, which reduces the T_g and modulus of the material. Carbon fabric is used to increase the strength of toughened SMP2-2. The DMA curves of different layers SMP2-2 based composites are shown in Fig. 4 (c-d). The storage modulus of shape memory BMI based composites is higher than that of SMP2-2, and the T_g of composites is lower than that

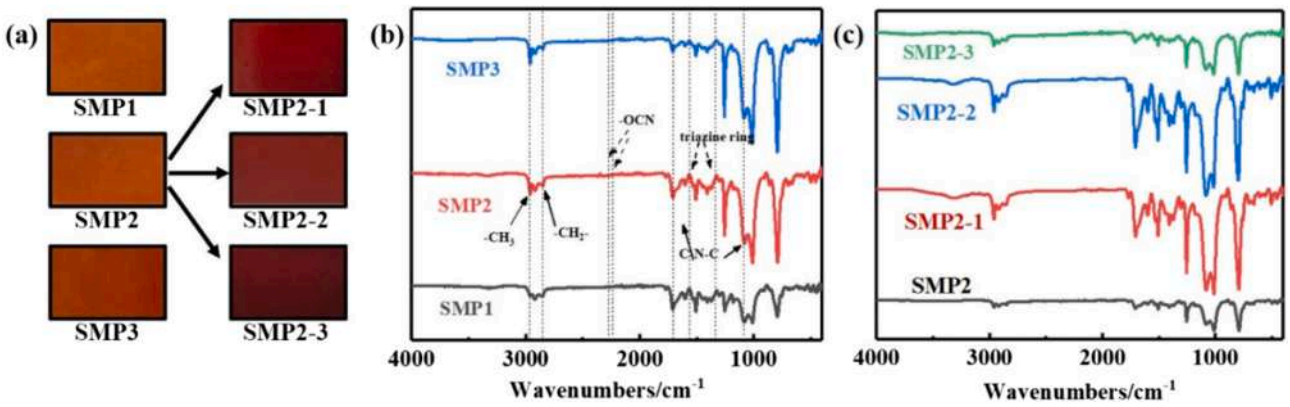

Fig. 2. Color of cured SMPs, FTIR spectra of (a) BMI-based SMPs with different mixture ratios and (b) SMPs with different nitrile rubber ratios.

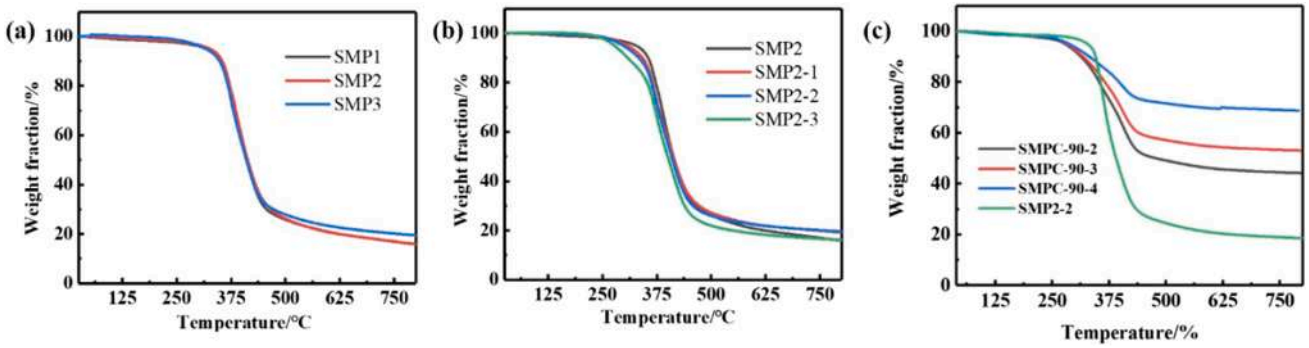

Fig. 3. Thermal performance of (a) BMI-based SMPs with different mixture ratios and (b) SMPs with different nitrile rubber ratios (c) SMP2-2 based composites and SMP2-2.

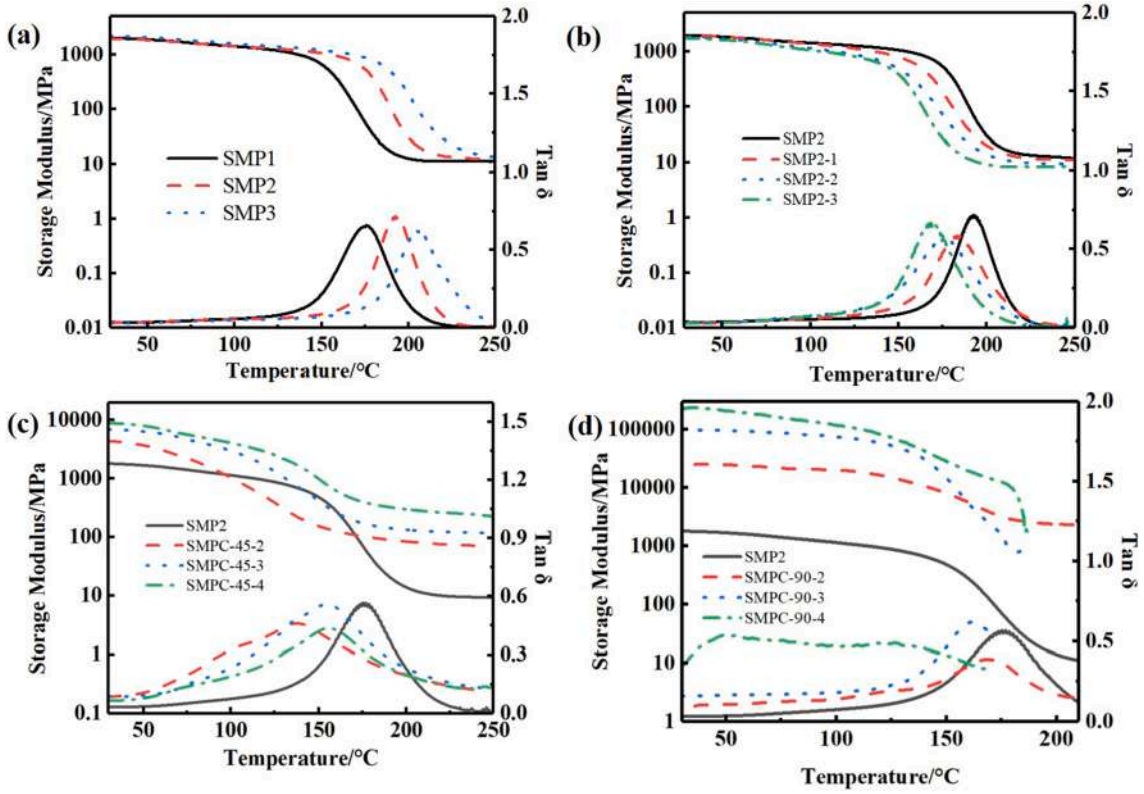

Fig. 4. DMA results in the tension of (a) BMI-based SMPs with different mixture ratios (b) SMPs with different ratios of ETBN and (c-d) SMP2-2 based composites and SMP2-2.

Table 2
DMA properties of BMI-based SMPs.

Sample	$E_{25°C}$/MPa	$E_{Tg-40°C}$/MPa	$E_{Tg+40°C}$/MPa	T_g/°C
SMP1	1992	1007	11.28	176
SMP2	1929	1015	12.84	193
SMP3	2237	1045	14.29	204
SMP2-1	1930	869.8	11.71	185
SMP2-2	1800	552.3	10.29	176
SMP2-3	1763	766.0	8.39	168
SMPC-90–2	24,941	13,921	2305	168
SMPC-90–3	87,179	56,058	–	162
SMPC-90–4	178,396	–	–	–
SMPC-45–2	4367	1106	100	138
SMPC-45–3	6566	2015	139	154
SMPC-45–4	8723	3136	310	156

of SMP. As the addition of carbon fabric makes the thermal conductivity of materials better, the materials response faster to temperature and exhibit lower T_g. The T_g of SMPC-90-4 did not been measure successfully, because the content of fiber in the material was relatively high and the content of resin was relatively low. In the DMA test, the polymer material became soft and was clamped at high temperature, but SMPC-90-4 slipped out as the resin content was low.

3.4. Static mechanical properties

Tensile test is used to evaluate the static mechanical properties of materials, and to assess indirectly the toughness of the material. The tensile stress–strain curves of BMI-based SMPs and SMPCs at room temperature are shown in Fig. 5 and Fig. 6. As shown in Fig. 5(a), the modulus of SMPs modified by TDI is different. This is because TDI forms an interpenetrating polymer network (IPN) with the BMI system, and the

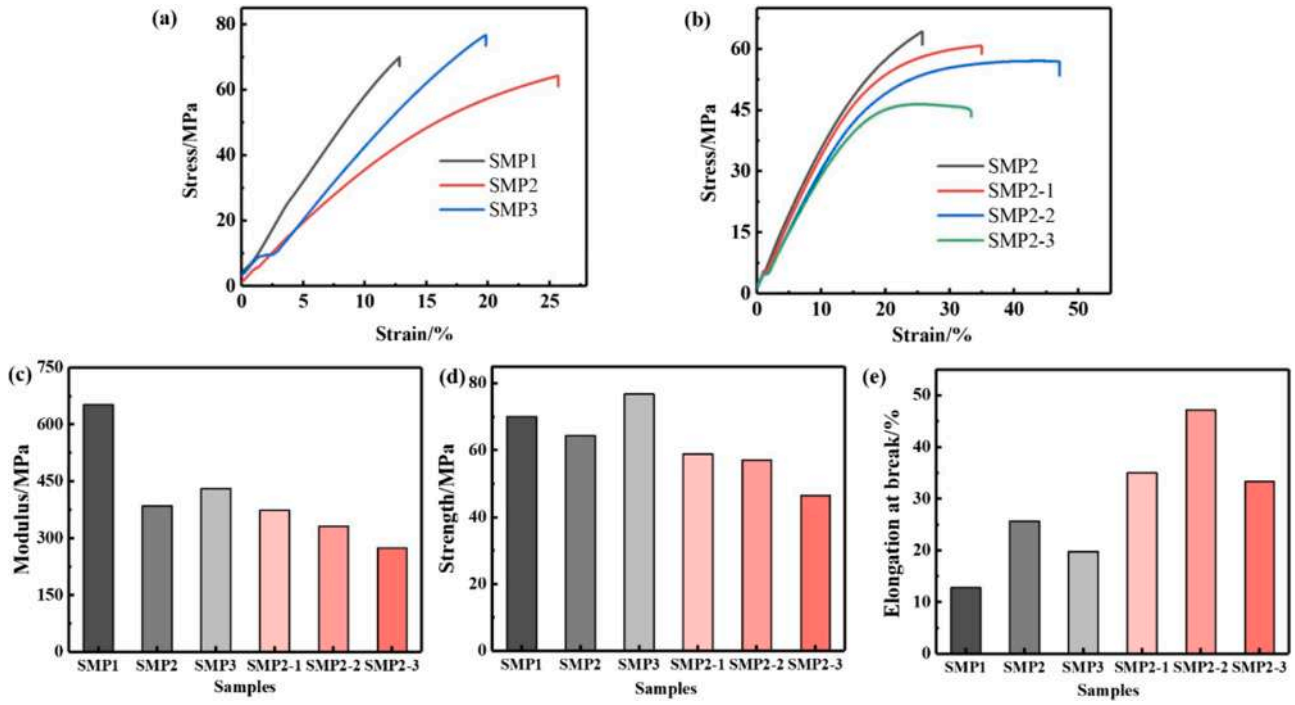

Fig. 5. Tensile stress–strain curves of (a) BMI-based SMPs with different mixture ratios (b) SMPs with different nitrile rubber ratios, and (c-e) elongation at break, strength and modulus variation of BMI-based SMPs.

flexibility of the system is improved. SMP2 showed the highest flexibility among BMI-based SMPs with different TDI ratios, so ETBN was added on the basis of SMP2. The modulus of SMP1 with the highest modulus is 651.5 MPa, and that of SMP2 with the lowest modulus is 385.4 MPa.

When five phr ETBN were added, ETBN was cross-linked with backbone structure. ETBN with more extended soft segment made the cross-linked system more ductile and longer elongation. The modulus of SMP2-2 is 331.1 MPa and the fracture elongation is 47.1 %, nearly doubled from 25.7 % of SMP2, as shown in Fig. 5(b). At the same time, the increase of soft segment is accompanied by the increase of cross-linking point, so the strength is unchanged. The addition of ETBN improved the toughness and elongation while ensuring stability. When more ETBN were added, the rubber phase formed by excessive ETBN gradually separated from the system and the rubber particle size increased. Although the strength of SMP2-3 is reduced due to the addition of rubber, the toughness of it is still improved with the modulus of 274.5 MPa. Fig. 5(c-e) illustrates the mechanical parameters comparison of BMI-based SMPs.

Fig. 6(a-b) shows the stress–strain curves of materials with different fiber layers and fiber direction. It can be seen from the curve of SMP2-2 and SMPCs that the curve first increases linearly and the material is in the linear elastic stage. From the microscopic point of view, the bonding length and the bonding angle of the polymer changed because the material was being stretched, but the bonding angle was not destroyed. After that, the stress and strain no longer maintain a linear relationship. From a microscopic perspective, the polymer molecular chains are gradually destroyed with macroscopic strain softening. After the molecular chains in the polymer are completely destroyed, the fiber continues to bear the load until the material is completely destroyed. With the addition of carbon fabric and the number of layers increase, the strength and modulus of composites increased significantly as shown in Fig, 6 (c-d). The elongation at break of the SMPC samples decreases to a certain extent as shown in Fig, 6 (e). The samples cut along the 0/90° direction of the carbon fabric have higher strength and modulus than that of ± 45° direction ones. Among these SMPCs, SMPC-45–3 achieved the effect of strengthening and toughening at the same time.

SEM micrographs of the fracture surface for BMI-based materials are shown in Fig. 7(a-g). The fracture surface of SMP1 is smooth, as shown in Fig. 7(a), which belongs to the typical brittle fracture. After adding more TDI in SMP2, the cross-section was staggered, and the crazes appeared as shown in Fig. 7(b). It indirectly indicated that the IPN system absorbs energy and forms stress concentration, which promotes the brittle-ductile transition and yielding, which lead to crazing. This indicates that the fracture mode of SMP2 was a ductile fracture.

After adding ETBN, the rubber phase gradually precipitates, forming small spheres dispersed in the resin matrix to form a “sea-island structure”. Rubber particles of different sizes in SMPs with different ETBN contents can be seen in Fig. 7(c,e-f). As the stress concentration point, the rubber phase will undergo deformation when subjected to an external force. They will absorb a large amount of deformation energy and induce the matrix shear yield to enhance the toughness of SMPs. The wrinkles at the fracture can be seen in Fig. 7(d,e). The rubber chain soft segment is cross-linked with the BMI backbone to form the rubber-BMI system. The rubber-BMI system is entangled with the TDI-BMI system, which results in the generation of wrinkles. This wrinkle also indicates the ductile fracture mode of the material. However, as shown in Fig. 7(f), there is no wrinkle on the fracture surface of the SMP with ETBN content of ten phr, which is compounded with excessive rubber phase and reduced material strength. Therefore, SMP2-2 with proper properties is selected for further composite research. The surface photograph of SMPC-45–2 before and after the tensile test is shown in Fig. 7(g-h). It can be seen in Fig. 7(i) that the fibers were bonded together by resin, which is consistent with the sufficient resin content of the composite.

3.5. *Shape memory properties*

As shape memory materials, the basic deformation abilities of these BMI-based materials were characterized by fixed rate, recovery rate and recovery speed. Fig. 8 shows the process of material deformation. The spline was bent into a “U” shape and deformed back to its original shape in one minute. This process is repeatable, and there are no obvious defects on the surface of the sample after deformation. All samples showed good fixation rate and recovery rate in the process of bending

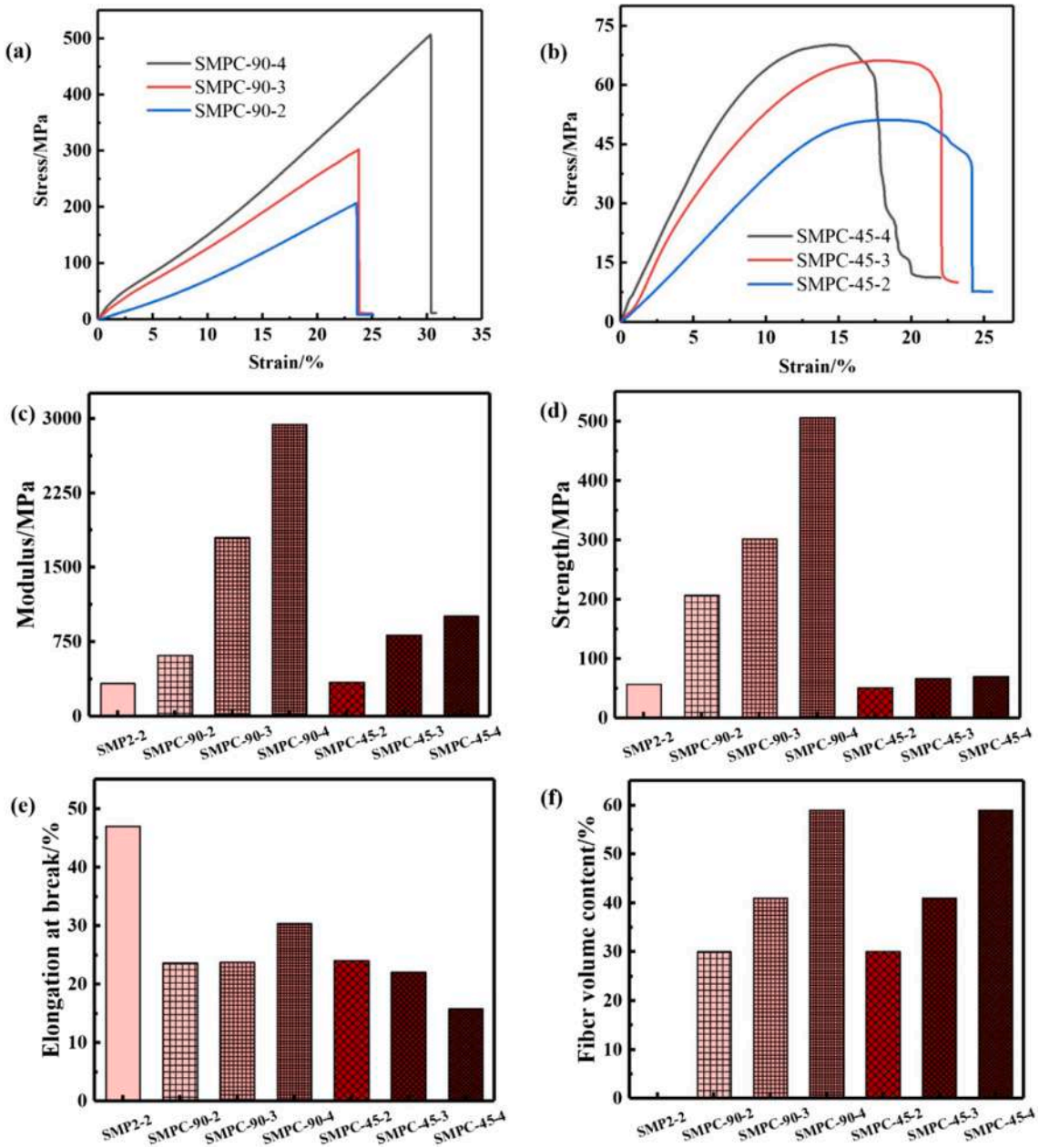

Fig. 6. Tensile stress–strain curves of (a) SMPCs with different layers of 0/90° direction carbon fabric (b) SMPCs with different layers of ± 45° direction carbon fabric, and (c-f) elongation at break, strength, modulus and fiber volume content variation of SMPCs.

deformation and recovery.

The five times shape memory cycle curve of all SMPs were shown in Fig. 9. After calculation, the fixing and recovery ratios of each SMP were shown in Table 3. Each sample showed good fixing and recovery rate. In the process of heating and cooling, the material showed slight strain less than 2 %, which is a normal phenomenon of thermal expansion and cold contraction. Among SMP1 ~ SMP3, SMP2 shows the highest fixing rate and recovery rate, so ETBN is added on the basis of SMP2. The recovery rate of SMP added with ETBN is slightly lower than that of SMP2, which is due to the addition of rubber phase. After five cycles, each SMP still maintained excellent fixing and recovery rate.

3.6. Demonstration of two-way performance

In this paper, we qualitatively demonstrated the two-way function of the shape memory bismaleimide and its composite through grasping objects. Figs. 10 and 11 show the two-way performance of SMP2 and SMPC-45–3, respectively. SMP2 was made into a collapsed grab structure as the initial shape, as shown in Figs. 10-S0. First, the structure was placed in an oven with a temperature of $T_g + 40$ °C for two minutes to be completely heated. At this time, the structure had been thoroughly softened. It was slowly arranged into a flat unfolded grasping structure, as shown in Figs. 10-S1. It was kept in a flat state and cooled to room temperature. Second, it was placed in an oven with a temperature of $T_g - 40$ °C for two minutes to be completely heated. The hardness of the structure was relatively hard at room temperature and relatively soft at $T_g + 40$ °C. Then it was arranged into a folded grab structure, as shown in Figs. 10-S2, and was cooled to room temperature. Third, place the folded grab structure in an oven at $T_g - 40$ °C. It takes 15 s for the test piece to recover from the temporary shape S2 to the first recovered shape $S1_{rec}$, which is a flat structure, as shown in Figs. 10-S1rec. Last, the recovered flat grab structure was placed in an oven at $T_g + 40$ °C. It reverted to the collapsed structure, as shown in Figs. 10-S2rec. The time taken for the recovered flat grab structure to recover from the first

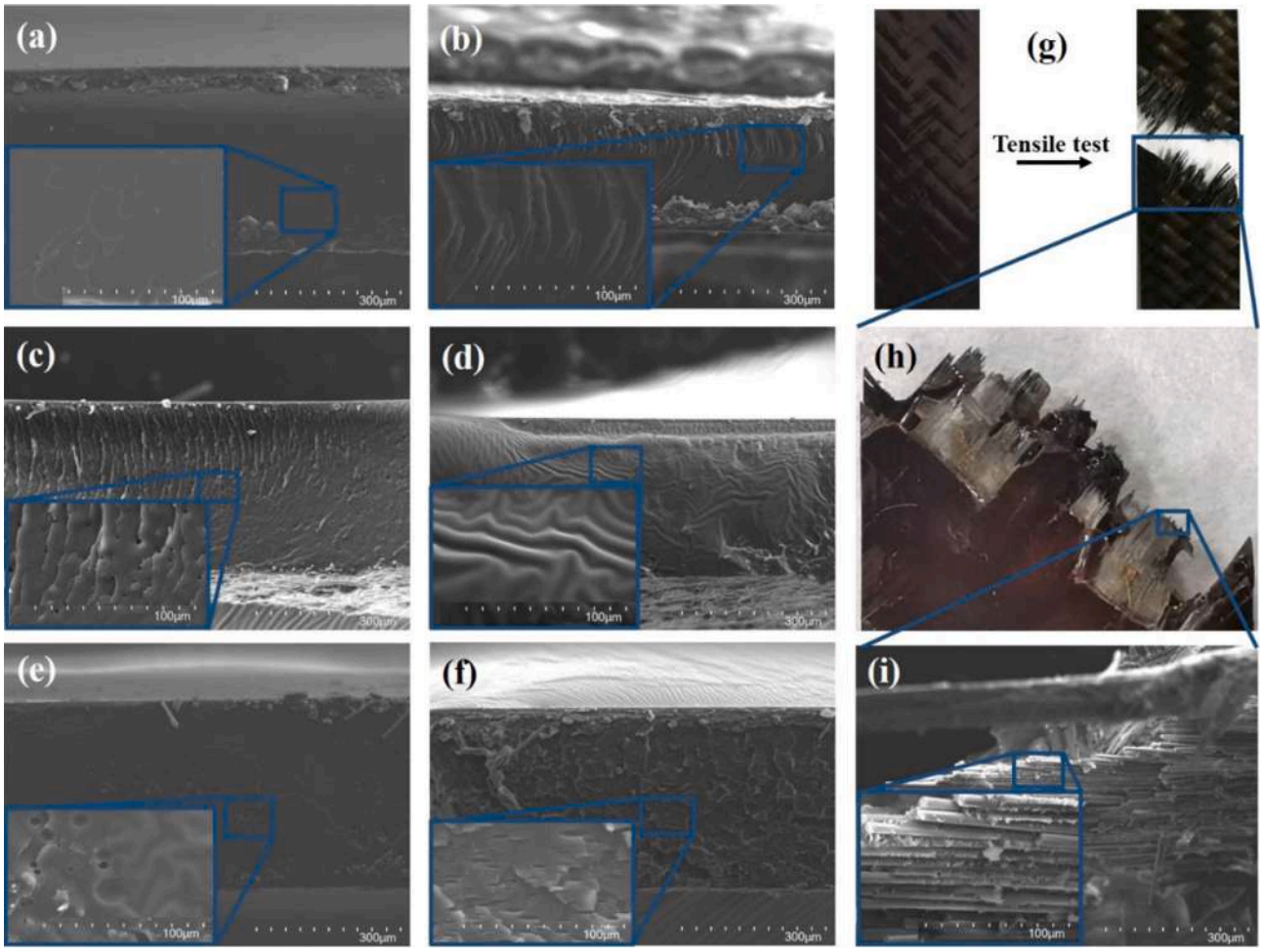

Fig. 7. SEM micrographs of the fracture surface for systems: (a) SMP1, (b) SMP2, (c-d) SMP2-1, (e) SMP2-2, (f)SMP2-3 and (i) SMPC-45–2. (g-h) Surface photograph of SMPC-45–2 before and after the tensile test.

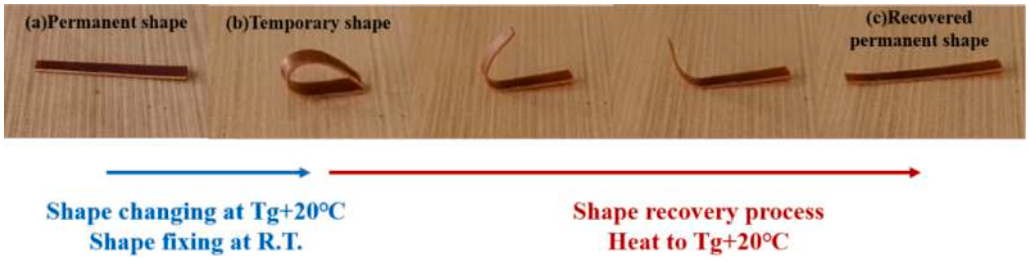

Fig. 8. Visual demonstration of SMP2-1′s dual-shape memory effect.

recovered shape $S1_{rec}$ to the second recovered shape $S2_{rec}$ is five seconds. Video. 1 and Video.2 show the first and the second shape recovery process of SMP2-2.

The structure of the SMPC-45–3 we made was a retractable claw with a width of 20 mm, as shown in Fig. 11-S0. First, the claw was placed in an oven with a temperature of T_g + 40 °C for two minutes to be completely heated. At this time, the claw had been wholly softened. And it was stretched out slowly, as shown in Fig. 11-S1. It was kept and cooled to room temperature. Second, it was placed in an oven with a temperature of T_g − 40 °C for two minutes to be completely heated. The hardness of the structure was relatively hard at room temperature and relatively soft at T_g + 40 °C. Then it was drawn back, as shown in Fig. 11-S2, and was cooled to room temperature. Third, place the retracted claw in an oven at T_g − 40 °C. It takes 45 s for the test piece to recover from the temporary shape S2 to the first recovered shape $S1_{rec}$, which is an extended claw, as shown in Fig. 11-S1rec. A rubber stopper was placed in the claw. The weight of the rubber stopper is about 250 g, which is 29.8 times of the 8.4 g claw structure. Last, the recovered extended claw with the stopper was placed in an oven at T_g + 40 °C. It reverted to the retracted claw in horizontal direction, as shown in Fig. 11-S2rec. The time taken for the claw to recover from the first recovered shape $S1_{rec}$ to the second recovered shape $S2_{rec}$ is 60 s. The second recovery process became slower. This is due to the rubber stopper being placed in the claw. The stopper has a certain reverse effect on the recovery of the claw. The shape recovery time of the composite was longer than that of BMI-based SMP, as the composite made in this research was thicker than the SMP. The heavier the structure, the slower the deformation process is slower. Video. 3 and Video.4 show the first and the second shape

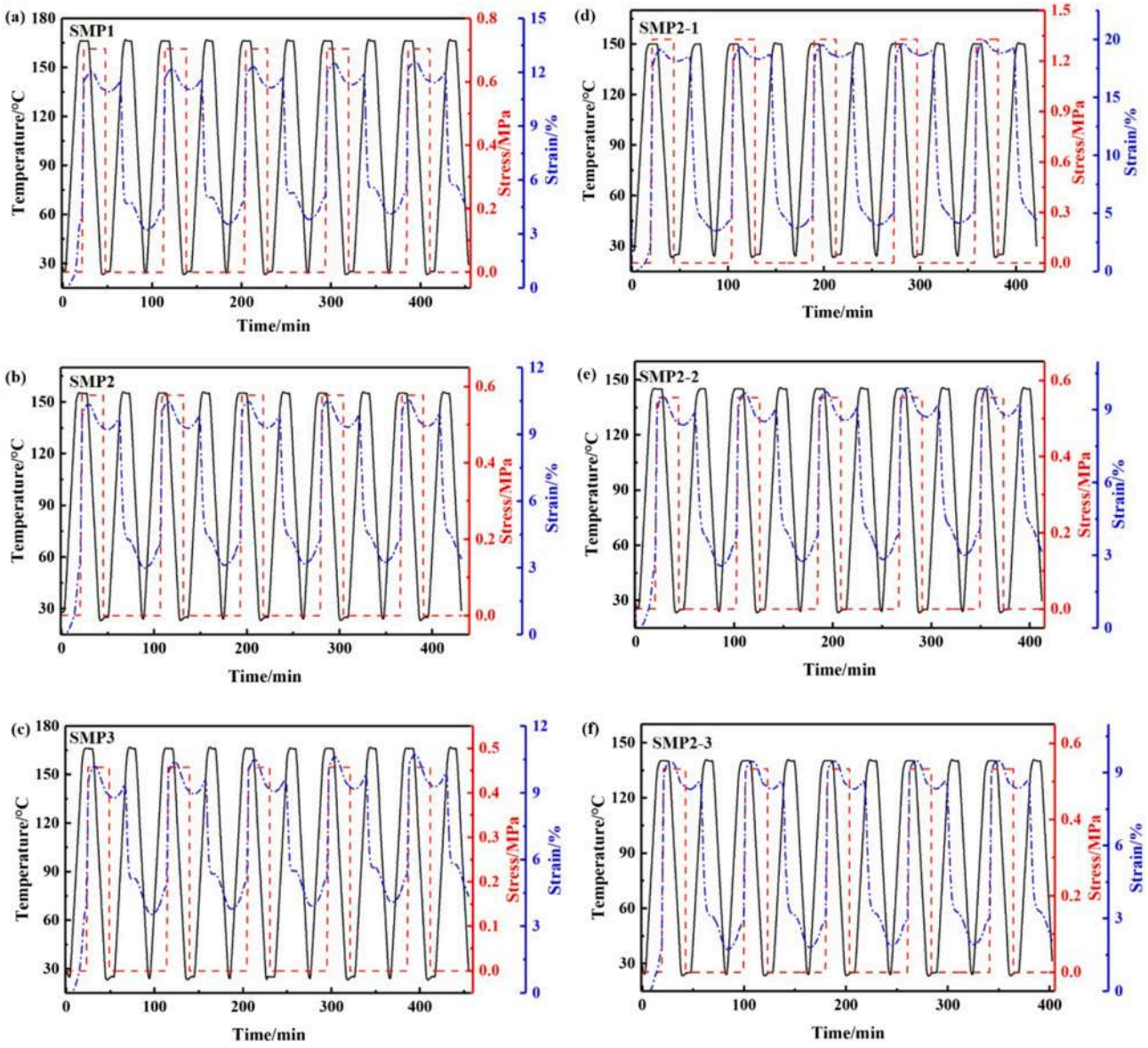

Fig. 9. Five times consecutive shape memory cycles curves of SMP1 (a), SMP2 (b), SMP3 (c), SMP2-1 (d), SMP2-2 (e), SMP2-3 (f).

Table 3
Fixing and recovery ratios of BMI-based SMPs.

Sample	SMP1	SMP2	SMP3	SMP2-1	SMP2-2	SMP2-3
R_f /%	99	99	99	99	99	99
R_r /%	91	96	94	93	93	95

recovery process of SMPC-45–3.

Generally, thermosetting shape memory polymers with narrow T_g peaks show dual-SME. This kind of SME can be explained by a two-phase mechanism. The crosslinking points in the polymer are regarded as permanent phase, which is used to fix the shape of SMP. Mobile molecular segments are considered a reversible phase, which is responsible for the deformation. However, the polymer with triple-SME generally has a wide T_g peak. The polymer network of that polymer is complex and has a variety of permanent and reversible phases, showing that the segments can be fixed and moved at different temperatures. Therefore, those polymers can remember the pre-deformed shape twice. By designing the second pre-deformed shape similar to the original shape, the two-way function can be realized. This kind of two-way performance is presented as the structure changes from the 'original' shape to the first pre-deformed shape and changes back to the original shape. This forms the two-way performance realized by programming.

4. Conclusions

A series of BMI-based SMPs were successfully synthesized. By adding chain extender polyether-amine, cross-linking agent cyanate-ester and rubber phase liquid nitrile rubber, the synergistic toughening was carried out to meet the needs of practical application. The infrared spectroscopy test proved that the required substance is generated. The highest temperature that the materials can be used are above 250 °C, which are higher than the T_g of the materials. The T_g ranges of the series of SMPs were indicated by DMA. Based on wide T_g ranges, the two-way function of those SMPs were realized by programming. The deformation temperature can be designed by adjusting the T_g from 168 °C to 204 °C, and two switching temperatures are $T_g \pm 40$ °C which can independently fix two opposite shapes to achieve two-way function. The composites preparation process was explored and the grabbing structure was designed using BMI-based SMP and composite. The composite structure

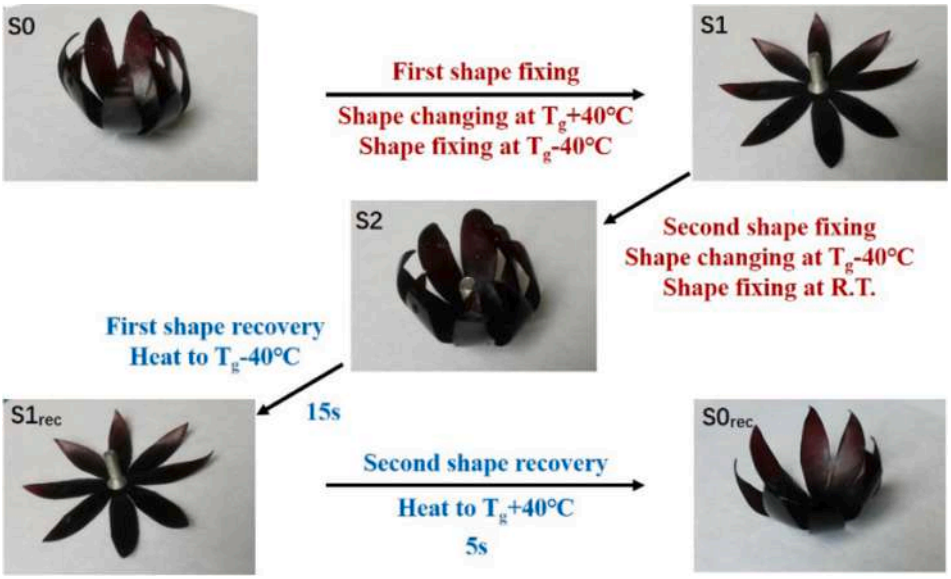

Fig. 10. Visual demonstration of SMP2-2′s two-way performance. S0: permanent shape; S1: first temporary shape (T_{d1}: T_g + 40 °C); S2: second temporary shape (T_{d2}: T_g − 40 °C); $S1_{rec}$: recovered first temporary shape (T_{r1}: T_g − 40 °C); $S0_{rec}$: recovered permanent shape (T_{r2}: T_g + 40 °C).

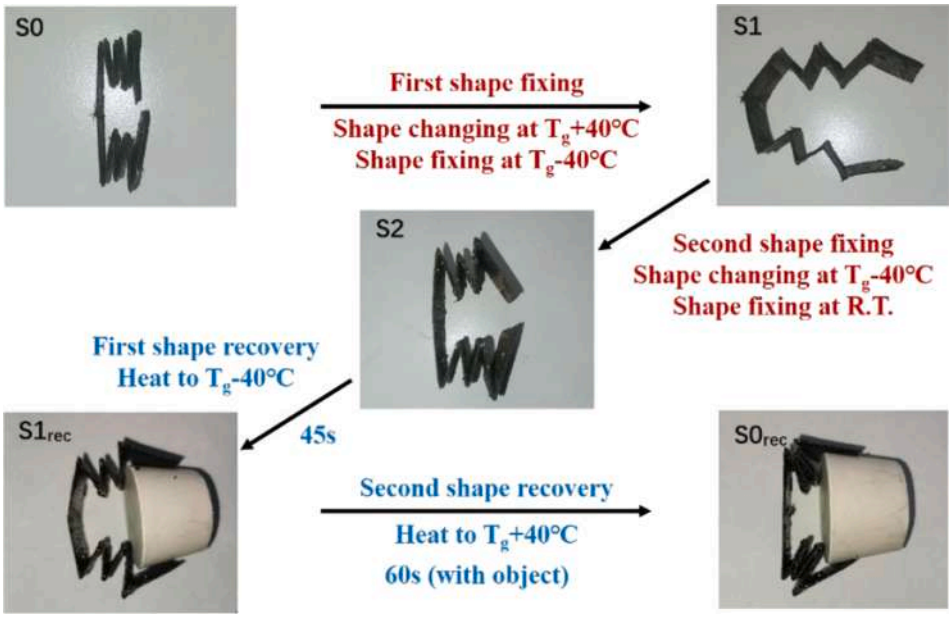

Fig. 11. Visual demonstration of SMPC-45-3′s two-way performance. S0: permanent shape; S1: first temporary shape (T_{d1}: T_g + 40 °C); S2: second temporary shape (T_{d2}: T_g-40 °C); $S1_{rec}$: recovered first temporary shape (T_{r1}: T_g-40 °C); $S0_{rec}$: recovered permanent shape (T_{r2}: T_g + 40 °C).

can grab 250 g items, which is 29.8 times of the 8.4 g claw structure.

CRediT authorship contribution statement

Yuejia Li: Investigation, Methodology, Data curation, Visualization, Writing – original draft, Writing – review & editing. **Fenghua Zhang:** Investigation, Methodology, Validation, Resources, Project administration, Writing – review & editing. **Yanju Liu:** Conceptualization, Supervision, Project administration, Funding acquisition, Writing – review & editing. **Jinsong Leng:** Conceptualization, Supervision, Project administration, Funding acquisition, Writing – review & editing.

Declaration of Competing Interest

The authors declare that they have no known competing financial interests or personal relationships that could have appeared to influence the work reported in this paper.

Data availability

Data will be made available on request.

Acknowledgements

This work is supported by the National Natural Science Foundation of China (Grant No. 11632005).

Appendix A. Supplementary data

Supplementary data to this article can be found online at https://doi.

org/10.1016/j.compositesa.2022.107328.

References

[1] Behl M, Lendlein A. Shape-memory polymers. Mater Today 2007;10(4):20–8.
[2] Leng J, Lan X, Liu Y, Du S. Shape-memory polymers and their composites: Stimulus methods and applications. Prog Mater Sci 2011;56(7):1077–135.
[3] Lendlein A, Kelch S. Shape-memory polymers. Angew Chem-Int Edit 2002;41(12):2034–57.
[4] Yu L, Yu H. Light-powered tumbler movement of graphene oxide/polymer nanocomposites. ACS Appl Mater Interfaces 2015;7(6):3834–9.
[5] Sahoo NG, Rana S, Cho JW, Li L, Chan SH. Polymer nanocomposites based on functionalized carbon nanotubes. Prog Polym Sci 2010;35(7):837–67.
[6] Lv H, Leng J, Liu Y, Du S. Shape-Memory Polymer in Response to Solution. Adv Eng Mater 2008;10(6):592–5.
[7] Li Y, Chen H, Liu D, et al. pH-Responsive Shape Memory Poly(ethylene glycol)-Poly (epsilon-caprolactone)-based Polyurethane/Cellulose Nanocrystals Nanocomposite. ACS Appl Mater Interfaces 2015;7(23):12988–99.
[8] Roy D, Cambre JN, Sumerlin BS. Future perspectives and recent advances in stimuli-responsive materials. Prog Polym Sci 2010;35(1–2):278–301.
[9] Liu C, Qin H, Mather PT. Review of progress in shape-memory polymers. J Mater Chem 2007;17(16):1543.
[10] Chen W, Zhu C, Gu X. Thermosetting polyurethanes with water-swollen and shape memory properties. J Appl Polym Sci 2002;84(8):1504–12.
[11] Dong Y, Ni Q-Q, Fu Y. Preparation and characterization of water-borne epoxy shape memory composites containing silica. Compos A Appl Sci Manuf 2015;72:1–10.
[12] Yu K, McClung AJW, Tandon GP, Baur JW, Jerry Qi H. A thermomechanical constitutive model for an epoxy based shape memory polymer and its parameter identifications. Mechanics of Time-Dependent Materials 2014;18(2):453–74.
[13] Li FK, Perrenoud A, Larock RC. Thermophysical and mechanical properties of novel polymers prepared by the cationic copolymerization of fish oils, styrene and divinylbenzene. Polymer 2001;42(26):10133–45.
[14] Zhao F, Zheng X, Zhou S, Zhou Bo, Xue S, Zhang Yi. Constitutive model for epoxy shape memory polymer with regulable phase transition temperature: Constitutive model for epoxy shape memory polymer with regulable phase transition temperature. Int J Smart Nano Mater 2021;12(1):72–87.
[15] Santhosh Kumar KS, Biju R, Reghunadhan Nair CP. Progress in shape memory epoxy resins. React Funct Polym 2013;73(2):421–30.
[16] Gu J, Zhang X, Duan H, Wan M, Sun H. A hygro-thermomechanical constitutive model for shape memory polymers filled with nano-carbon powder. Int J Smart Nano Mater 2021;12(3):286–306.
[17] Serrano MC, Carbajal L, Ameer GA. Novel biodegradable shape-memory elastomers with drug-releasing capabilities. Adv Mater 2011;23(19):2211–5.
[18] Kunzelman J, Chung T, Mather PT, Weder C. Shape memory polymers with built-in threshold temperature sensors. J Mater Chem 2008;18(10):1082.
[19] Khaldi A, Plesse C, Vidal F, Smoukov SK. Smarter actuator design with complementary and synergetic functions. Adv Mater 2015;27(30):4418–22.
[20] Hu J, Chen S. A review of actively moving polymers in textile applications. J Mater Chem 2010;20(17):3346.
[21] Lan X, Liu Y, Lv H, Wang X, Leng J, Du S. Fiber reinforced shape-memory polymer composite and its application in a deployable hinge. Smart Mater Struct 2009;18(2):024002.
[22] Li YueJia, Zhang FengHua, Liu YanJu, Leng JinSong. 4D printed shape memory polymers and their structures for biomedical applications. Sci China-Technol Sci 2020;63(4):545–60.
[23] Zhao Q, Qi HJ, Xie T. Recent progress in shape memory polymer: New behavior, enabling materials, and mechanistic understanding. Prog Polym Sci 2015;49–50:79–120.
[24] Xie T. Tunable polymer multi-shape memory effect. Nature 2010;464(7286):267–70.
[25] Dolog R, Weiss RA. Shape memory behavior of a polyethylene-based carboxylate ionomer. Macromolecules 2013;46(19):7845–52.
[26] NöCHEL U, Kumar u n, wang k,, et al. Triple-shape effect with adjustable switching temperatures in crosslinked poly[ethylene-co-(vinyl acetate)]. Macromol Chem Phys 2014;215(24):2446–56.
[27] Bellin I, Kelch S, Langer R, Lendlein A. Polymeric triple-shape materials. Proc Natl Acad Sci USA 2006;103(48):18043–7.
[28] Torbati AH, Nejad HB, Ponce M, Sutton JP, Mather PT. Properties of triple shape memory composites prepared via polymerization-induced phase separation. Soft Matter 2014;10(17):3112–21.
[29] Luo X, Mather PT. Triple-shape polymeric composites (TSPCs). Adv Funct Mater 2010;20(16):2649–56.
[30] Xie T, Xiao X, Cheng YT. Revealing triple-shape memory effect by polymer bilayers. Macromol Rapid Commun 2009;30(21):1823–7.
[31] Li G, Xu W. Thermomechanical behavior of thermoset shape memory polymer programmed by cold-compression: Testing and constitutive modeling. J Mech Phys Solids 2011;59(6):1231–50.
[32] Li G, King A, Xu T, Huang X. Behavior of thermoset shape memory polymer-based syntactic foam sealant trained by hybrid two-stage programming. J Mater Civ Eng 2013;25(3):393–402.
[33] Zhang Q, Wei H, Liu Y, Leng J, Du S. Triple-shape memory effects of bismaleimide based thermosetting polymer networks prepared via heterogeneous crosslinking structures. RSC Adv 2016;6(13):10233–41.
[34] Nair C. Advances in addition-cure phenolic resins. Prog Polym Sci 2004;29(5):401–98.
[35] Biju R, Nair CPR. High transition temperature shape memory polymer composites based on bismaleimide resin. High Perform Polym 2013;25(4):464–74.
[36] Shen ZW, Schlup JR, Fan LT. Synthesis and characterization of leather impregnated with bismaleimide (BMI) - Jeffamine (R) resins. J Appl Polym Sci 1998;69(5):1019–27.
[37] Luo C, Zhang B, Zhang W, Yuan C, Dunn M, Ge Qi, et al. Chemomechanics of dual-stage reprocessable thermosets. J Mech Phys Solids 2019;126:168–86.
[38] Bell CL, Peppas NA. Equilibrium and dynamic swelling of polyacrylates. Polym Eng Sci 1996;36(14):1856–61.
[39] Shumaker JA, McClung AJW, Baur JW. Synthesis of high temperature polyaspartimide-urea based shape memory polymers. Polymer 2012;53(21):4637–42.
[40] Kannurpatti AR, Anseth JW, Bowman CN. A study of the evolution of mechanical properties and structural heterogeneity of polymer networks formed by photopolymerizations of multifunctional (meth)acrylates. Polymer 1998;39(12):2507–13.